A New Method for Determining the Nusselt and Sherwood Numbers in Simultaneous Heat and Mass Transfer in Solar Collector/Regenerators

Fernando Manuel Gómez Castro[1], Ursula Eicker[2], Ulrike Jordan[1]

[1] Institute for Thermal Engineering, Kassel University, Kassel (Germany)

[2] Next-Generation Cities Institute, Concordia University Montreal, Montreal (Canada)

Abstract

This paper presents a new method to evaluate Nusselt and Sherwood numbers for solar collector/regenerators. The method is based on dimensionless groups of the thermophysical properties, temperature and mass concentration gradients, heat and mass transfer coefficients and system geometry. The resulting relations for the Nusselt and Sherwood numbers are reliable to obtain good results of the coupled heat and mass exchange within forced-flow direct collector/regenerators. Unlike conventional relations, these are general expressions valid for different liquid desiccants. In this study the relations are validated with own measurements and with relations from literature.

Keywords: Nusselt number, Sherwood number, collector/regenerators, coupled heat and mass exchanges, liquid desiccants

1. Introduction

The overall performance of a direct solar regenerated liquid desiccant system strongly depends on the solar collector/regenerator (C/R), which adjusts the mass fraction of the hygroscopic solution used for dehumidifying air. A detailed understanding of the coupled heat and mass fluxes at the liquid-gas interface in the C/R is required to derive new correlations for the Nusselt and Sherwood numbers for refining the accuracy of computations.

Yang and Wang (1994) derived empirical correlations for the Nusselt and Sherwood numbers in a 2 m width × 9 m length single-glazed counter-current C/R in the humid climate of Kaohsiung, Taiwan, and analysed the impact of operating conditions on the water desorption rate of both forced- and natural-flow C/Rs with a parameter study. Their results indicate that the forced convection C/R outperforms the natural convection one at low mass fractions of lithium chloride (LiCl).

Li and Yang (2010) conducted laboratory-scale tests with a 1 m width × 2 m length single-glazed parallel-flow C/R for assessing the effects of parameters on the regeneration of an aqueous lithium bromide (LiBr) solution. Although high air mass flow rates improved the C/R performance at high solar irradiances, it was better to keep low air flow rates at cloudy conditions. Besides, empirical correlations for the heat and mass transfer coefficients were proposed as functions of the solar irradiance, the temperature, humidity ratio and mass flow rate of the air plus the temperature and mass fraction of the solution.

Finally, Peng and Zhang (2016) studied experimentally the regeneration process in a 1 m width × 2 m length single-glazed counter-flow solar C/R in terms of the inlet conditions of the air and aqueous LiCl solution and weather conditions in Southern China. They observed an optimal air flow rate that maximised the regeneration efficiency, whose value decreased by rising the flow rate of the solution at near ambient temperature, whereas the inverse trend was obtained at moderate solution temperature. They also proposed correlations for the Nusselt and Sherwood numbers with the Reynolds number, Prandtl and Schmidt numbers, inlet solution mass fraction, solution-to-air mass flow rate ratio and air-to-solution temperature ratio as arguments.

The correlations resulting from the above-mentioned researches are, nevertheless, only suitable for a specific liquid sorbent under transitional and turbulent air flow in the C/R channel. This paper presents general equations for the coupled dimensionless heat and mass transfer coefficients valid for aqueous solutions of $CaCl_2$, LiCl and LiBr obtained from both, own measurements and experimental data of Alizadeh and Saman (2002), Li and Yang

Selection and/or peer review under responsibility of Scientific Committee
doi:10.18086/eurosun.2022.06.06 Available at http://proceedings.ises.org

(2010), and Peng and Zhang (2015; 2016).

2. Description of the test rig

The tests were performed in the lab-scale arrangement comprising a forced-flow regenerating panel operating in counter-current mode with respect to aqueous calcium chloride ($CaCl_2$) trickling on its heat collecting surface, fans, solution tanks, pumps, flow regulator/indicator, PID controller and data acquisition devices. The single-pass single-glazed C/R consists of a transparent cover and a housing made of Plexiglas and is thermally insulated from its surroundings via 25 mm thick polystyrene sheets. Its tilt angle from the horizontal plane can be variably set from 15° to 30°. This device has a total area of 2.4 m² (1 m width × 2.4 m length), a sprinkling area of 2 m² (1 m width × 2 m length) and a gap height of 10 cm (see Fig. 1(a)). A black cotton fabric is used for ensuring both high absorption of solar irradiance and uniform wetting. The distribution of the hygroscopic liquid is carried out from top of the C/R via a drip system. The regenerating air enters the device through a circular inlet located in the centre of a lower distribution box. For a preferably even air streaming profile in the channel, 12 flow openings are distributed over the entire width of the inlet and outlet ports as shown in Fig. 1(b).

(a) C/R prototype (b) Air distribution chamber

Fig. 1: Free-standing collector/regenerator.

3. Instrumentation and experimental setup

Fig. 2 depicts the test rig of the direct solar regeneration unit with the installed measurement and system technology, which comprises subsystems for supplying forced air and for circulating and storing desiccant solution. The regenerating air is provided by an axial fan with continuous flow control in the range of 50 to 250 m³/h, whereas the weak $CaCl_2$ solution is delivered to a PVC liquid distributor header (located at the top of the C/R) with symmetrically arranged openings with an inner diameter of 0.7 mm and a separation distance of 1 cm by a plastic solution pump at volumetric flow rates between 5 and 30 l/h. The temperature of the incoming solution to the C/R is controlled by the combination of an ARCTIC cold bath/circulation thermostat HAAKE AC 150-A10 and a plate heat exchanger B3-12A-30-2.0. The strong hygroscopic liquid is then collected in a gutter and pumped back to a PVC solution tank. The volumetric flow rates and temperatures of the fluids, air relative humidity and solution density are measured at the inlet and outlet of the C/R once the fluids conditions approach steady-state.

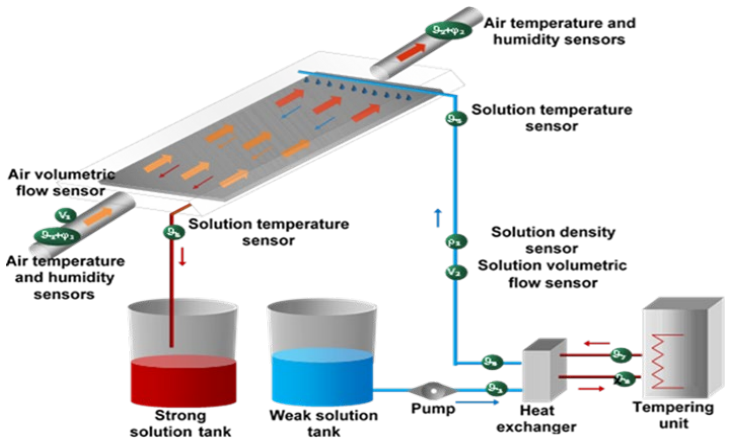

Fig. 2: System sketch of the C/R prototype.

4. Calculation of Nusselt and Sherwood numbers from experimental data

The convective heat and mass transfer coefficients in the gas-phase streaming within the C/Rs have been determined from data both, measured in the test rig and published by Alizadeh and Saman (2002), Li and Yang (2010) and Peng and Zhang (2015; 2016) with the logarithmic mean difference method:

$$h_{Conv,s\text{-}a} = \dot{m}_{da} \cdot c_{p,a} \cdot \left(T_{a,out} - T_{a,in}\right) / \left(A_s \cdot \Delta T_{LM,s\text{-}a}\right) \quad \text{(eq. 1)}$$

$$h_{Conv,mD,s\text{-}a} = \dot{m}_{da} \cdot \left(\chi_{a,out} - \chi_{a,in}\right) / \left(A_s \cdot \Delta \rho_{LM,s\text{-}a}\right) \quad \text{(eq. 2)}$$

With $\dot{m}_{da}$ as the mass flow rate of the dry air and $c_{p,a}$ as the isobaric specific heat capacity of the moist air; ($T_{a,out}$, $\chi_{a,out}$) and ($T_{a,in}$, $\chi_{a,in}$) as the pairs of the temperatures and humidity ratios of the air at the top and bottom of the counter-flow C/R; A_s as the area of the liquid sorbent; $\Delta T_{LM,s\text{-}a}$ and $\Delta \rho_{LM,s\text{-}a}$ as the logarithmic mean temperature and mass concentration differences at the liquid-air interface, which are given by:

$$\Delta T_{LM,s\text{-}a} = \left(T_{a,out} - T_{a,in}\right) / \left(Ln\left(T_s - T_{a,in}\right) - Ln\left(T_s - T_{a,out}\right)\right) \quad \text{(eq. 3)}$$

$$\Delta \rho_{LM,s\text{-}a} = \left(\rho_{a,out} - \rho_{a,in}\right) / \left(Ln\left(\rho_s - \rho_{a,in}\right) - Ln\left(\rho_s - \rho_{a,out}\right)\right) \quad \text{(eq. 4)}$$

Where are T_s and ρ_s are the temperature and mass concentration of water vapour of the desiccant solution.

The dimensionless heat transfer coefficient, the Nusselt number ($Nu_{s\text{-}a,Dh}$), is then defined as:

$$Nu_{s\text{-}a,Dh} = h_{Conv,s\text{-}a} \cdot D_h / k_a \quad \text{(eq. 5)}$$

With D_h as the hydraulic diameter of the air channel and k_a as the thermal conductivity of the moist air.

The dimensionless mass transfer coefficient, the Sherwood number ($Sh_{s\text{-}a,Dh}$), is given by:

$$Sh_{s\text{-}a,Dh} = h_{Conv,mD,s\text{-}a} \cdot D_h / D_{12} \quad \text{(eq. 6)}$$

Where D_{12} is the diffusivity of water vapour in the air.

5. Proposed approach

The comprehensive database of Nusselt and Sherwood numbers evaluated from both the measurements in previously described test rig and the experimental results extracted from Alizadeh and Saman (2002), Li and Yang (2010) and Peng and Zhang (2015; 2016) has been used to derive new empirical correlations for assessing the heat and mass exchanges within the C/R. In simultaneous heat and mass transfer, the Nusselt and Sherwood numbers are influenced by several major parameters including the thermophysical properties of the liquid and gas phases, latent heat of evaporation and specific enthalpy of dilution during phase change, temperature and mass concentration gradients due to the phase change, single-phase convective heat and mass transfer coefficients, gravitational acceleration and system geometry:

$$Nu_{s\text{-}a,D_h}=f\left(\rho_a,\mu_a,\beta_a,c_{p,a},k_a,\beta_{c,a},D_{12},h_a,u_a,\rho_s,\mu_s,\sigma_s,u_s,h_{fg}+h_{Dil},\Delta T_{s\text{-}a},\Delta\rho_{s\text{-}a},h_{Conv,s\text{-}a,0},g\cdot Sin(I_c),D_h,L_p,\delta_s\right) \quad \text{(eq. 7)}$$

$$Sh_{s\text{-}a,D_h}=f\left(\rho_a,\mu_a,\beta_a,c_{p,a},k_a,\beta_{c,a},D_{12},h_a,u_a,\rho_s,\mu_s,\sigma_s,u_s,h_{fg}+h_{Dil},\Delta T_{s\text{-}a},\Delta\rho_{s\text{-}a},h_{Conv,mD,s\text{-}a,0},g\cdot Sin(I_c),D_h,L_p,\delta_s\right) \quad \text{(eq. 8)}$$

Consequently, eqs. 7 and 8 comprise 21 variables with 4 primary dimensions (i.e. kg [M], m [L], s [t], K [T]). Based on the dimensional analysis, 17 dimensionless parameters should be required in both the Nusselt and Sherwood number correlations, which can be reduced to the following pre-defined dimensionless numbers:

Dimensionless parameters for the Nusselt number correlation:

$$Re_{a,Dh}=\frac{u_a\cdot D_h}{\nu_a} \qquad Gr_{a,ch,Dh}=\left|\frac{g\cdot\beta_a\cdot\Delta T_{s\text{-}a}\cdot {D_h}^3}{{\nu_a}^2}\right|\cdot\left(\frac{D_h}{L_p}\right)\cdot Sin(I_c)$$

$$Le_{a,ev}=Le_a\cdot\left(\frac{h_{fg}+h_{Dil}}{h_a}\right) \qquad Ka_s=\left(\frac{\rho_s\cdot{\sigma_s}^3}{g\cdot Sin(I_c)\cdot{\mu_s}^4}\right)^{1/3}$$

$$Re_s^*=\frac{4\cdot u_s\cdot\delta_s}{\nu_s}$$

$$Nu_{s\text{-}a,Dh,0}=\frac{h_{Conv,s\text{-}a,0}\cdot D_h}{k_a} \qquad Gr_{a,m,ch,Dh}=\left|\frac{g\cdot\beta_{m,a}\cdot\Delta\rho_{s\text{-}a}\cdot {D_h}^3}{{\nu_a}^2}\right|\cdot\left(\frac{D_h}{L_p}\right)\cdot Sin(I_c) \quad \text{(eq. 9)}$$

Where $Re_{a,Dh}$ is the gas-phase Reynolds number (ratio of the inertial forces to viscous ones in the gas-phase); $Gr_{a,ch,Dh}$ is the channel thermal Grashof number (ratio of thermal buoyant forces to viscous ones acting on the gas-phase); $Le_{a,ev}$ is the Lewis number of evaporation for the gas-phase (product of the Lewis number and the enthalpy ratio), firstly introduced by Enayatollahi et al. (2017); Ka_s is the liquid-phase Kapitza number (ratio of surface tension forces to inertial ones in the liquid-phase); Re_s* is the liquid-phase Reynolds number (ratio of the inertial forces to viscous ones in the liquid-phase); $Gr_{a,m,ch,Dh}$ is the channel solutal Grashof number (ratio of solutal buoyant forces to viscous ones acting on the gas-phase) and $Nu_{s\text{-}a,Dh,0}$ is the single-phase Nusselt number.

Dimensionless parameters for the Sherwood number correlation:

The dimensionless parameter $Nu_{s\text{-}a,Dh,0}$ is substituted with the single-phase Sherwood number $Sh_{s\text{-}a,Dh,0}$.

The formulations are developed by logarithmically normalising the dimensionless groups with respect to their corresponding limits as suggested by Larachi and Levesque (2008). The Nusselt number for coupled heat and mass exchanges ($Nu_{s\text{-}a,Dh}$) at the liquid-air interface is given as the sum of the components for sensible ($Nu_{s\text{-}a,Dh,s}$) and latent ($Nu_{s\text{-}a,Dh,l}$) heat transfer (Cherif et al., 2011):

$$Nu_{s\text{-}a,Dh}=Nu_{s\text{-}a,Dh,s}+Nu_{s\text{-}a,Dh,l} \quad \text{(eq. 10)}$$

Here, $Nu_{s\text{-}a,Dh,s}$ is assessed from conventional expressions for the single-phase Nusselt number in a channel ($Nu_{s\text{-}a,Dh,0}$), e.g. Gnielinski (2010) for laminar flow and Taler (2017) for turbulent one, whereas $Nu_{s\text{-}a,Dh,l}$ is defined as:

$$Nu_{s\text{-}a,Dh,l}=(-0.905+11.467\cdot S)\cdot Nu_{s\text{-}a,Dh,0} \quad \text{(eq. 11)}$$

The normalised output function S is obtained from the following expression:

$$S=LR1+\sum_{i=1}^{7}LR2_i+\sum_{i=1}^{7}LR3_i \quad \text{(eq. 12)}$$

The auxiliary functions for the multiple linear regressions without interaction terms (LR1), with two-way interaction terms ($LR2_i$) and with three-way interaction terms ($LR3_i$) are defined as:

$$LR1=a_0+\sum_{i=1}^{7}a_i\cdot U_i \quad \text{(eq. 13)}$$

$$LR2_i=U_i\cdot\sum_{j=1}^{8-i}b_{i,j}\cdot U_{j+(i-1)} \quad 1\le i\le 7 \quad \text{(eq. 14)}$$

$$LR3_i=U_i^2\cdot\sum_{j=1}^{7}c_{i,j}\cdot U_j \quad 1\le i\le 7 \quad \text{(eq. 15)}$$

With their normalised inputs (U_i) and their ranges of validity given below:

$$U_1=\frac{Log\left(\frac{Re_{a,Dh}}{142.252}\right)}{4.675} \qquad U_2=\frac{Log\left(\frac{Gr_{a,ch,Dh}}{112.33}\right)}{8.839} \qquad U_3=\frac{Log\left(\frac{Le_{a,ev}}{19.529}\right)}{1.552}$$

$$U_4=\frac{Log\left(\frac{Ka_s}{288.24}\right)}{3.15} \qquad U_5=\frac{Log\left(\frac{Re_s^*}{0.773}\right)}{4.691} \qquad U_6=\frac{Log\left(\frac{Gr_{a,m,ch,Dh}}{458.766}\right)}{6.26}$$

$$U_7=\frac{Log\left(\frac{Nu_{s\text{-}a,Dh,0}}{23.957}\right)}{1.313} \quad \text{(eq. 16)}$$

Domain of applicability:

$142.252 \leq Re_{a,Dh} \leq 1.525 \cdot 10^4$ $112.33 \leq Gr_{a,ch,Dh} \leq 7.75 \cdot 10^5$
$19.529 \leq Le_{a,ev} \leq 92.204$ $288.24 \leq Ka_s \leq 6723.739$
$0.773 \leq Re_s^* \leq 84.273$
$23.957 \leq Nu_{s\text{-}a,Dh,0} \leq 89.011$ $458.766 \leq Gr_{a,m,ch,Dh} \leq 2.4 \cdot 10^5$

The numerical values of coefficients a_i, $b_{i,j}$ and $c_{i,j}$ in eqs. 13-15 for the transitional and turbulent air flow regimes are presented in Tab. 1.

Tab. 1: Coefficients a_i, $b_{i,j}$ and $c_{i,j}$ of the normalised output function for computing the Nusselt number in solar C/Rs according to the coupled calculation approach ($Re_{a,Dh} \geq 2300$).

a_i	0	1	2	3	4	5	6	7
	-5.871	52.179	17.256	18.346	-28.291	10.54	-41.606	-49.969
$b_{i,j}$	**0**	**1**	**2**	**3**	**4**	**5**	**6**	**7**
1		-29.103	-140.65	12.651	-0.006	-39.327	93.66	59.98
2		29.778	13.005	42.779	1.367	11.231	30.584	
3		-42.305	-13.642	-3.914	-18.839	25.694		
4		18.459	-15.537	-4.337	45.935			
5		14.552	4.884	-8.342				
6		23.421	-40.896					
7		10.908						
$c_{i,j}$	**0**	**1**	**2**	**3**	**4**	**5**	**6**	**7**
1		-8.931	85.955	-36.57	4.941	32.539	-37.092	-29.949
2		2.438	-7.356	-31.329	-49.056	19.557	5.869	2.438
3		41.616	16.256	-0.277	7.261	3.181	14.112	-23.01
4		5.371	24.736	2.741	-10.783	0.917	-18.798	-42.38
5		-5.621	-27.108	1.309	11.087	-4.773	9.019	21.173
6		-41.785	-10.22	14.051	26.282	-13.327	-9.081	33.897
7		14.405	-35.095	-3.449	-13.391	-20.337	11.934	4.918

The procedure outlined in eqs. 10-15 is called the coupled evaluation method, since it includes dimensionless parameters corresponding to both the temperature and concentration gradients, i.e. U_2 and U_6 (see eq. 16), as expected in simultaneous heat and mass transfer processes. Similarly, the Sherwood number for simultaneous heat and mass transfer processes ($Sh_{s\text{-}a,Dh}$) at the liquid-air interface is assessed in terms of the component obtained by applying the heat/mass transfer analogy to the single-phase Nusselt number ($Sh_{s\text{-}a,Dh,0}$) and the convection contribution due to phase change ($Sh_{s\text{-}a,Dh,l}$) as follows:

$$Sh_{s\text{-}a,Dh} = Sh_{s\text{-}a,Dh,0} + Sh_{s\text{-}a,Dh,l} \quad \text{(eq. 17)}$$

Where the component $Sh_{s\text{-}a,Dh,l}$ is given by:

$$Sh_{s\text{-}a,Dh} = (-0.733 + 11.161 \cdot S) \cdot Sh_{s\text{-}a,Dh,0} \quad \text{(eq. 18)}$$

With the normalised output function S and auxiliary functions LR1, $LR2_i$ and $LR3_i$ already defined by eqs. 12-15. Only the normalised input U_7 changes:

$$U_7 = \frac{Log\left(\frac{Sh_{s-a,Dh,0}}{23.127}\right)}{1.28} \quad \text{(eq. 19)}$$

Domain of applicability:

$23.127 \leq Sh_{s\text{-}a,Dh,0} \leq 83.189$

In this case, the coefficients a_i, $b_{i,j}$ and $c_{i,j}$ in eqs. 13-15 for the transitional and turbulent air flow regimes are summarised in Tab. 2.

Tab. 2: Coefficients a_i, $b_{i,j}$ and $c_{i,j}$ of the normalised output function for calculating the Sherwood number in solar C/Rs according to the coupled evaluation method ($Re_{a,Dh}$≥2300).

a_i	0	1	2	3	4	5	6	7
	29.79	-23.657	-88.397	-6.121	-1.497	-12.306	-23.806	35.304
$b_{i,j}$	**0**	**1**	**2**	**3**	**4**	**5**	**6**	**7**
1		45.896	17.759	31.526	-88.239	1.292	55.27	-10.944
2		50.09	9.419	91.958	3.028	79.645	-29.584	
3		-9.558	-6.018	2.72	-15.502	8.253		
4		5.111	12.751	-21.025	-63.391			
5		7.078	-2.297	14.395				
6		-11.28	-14.142					
7		-49.812						
$c_{i,j}$	**0**	**1**	**2**	**3**	**4**	**5**	**6**	**7**
1		-55.795	56.915	-31.063	79.57	-8.884	-38.248	11.133
2		-77.33	31.253	-10.724	-11.79	4.499	-83.69	19.426
3		9.86	-1.488	2.853	-0.029	0.522	7.715	-10.426
4		8.003	-56.905	8.312	0.116	-0.346	16.286	29.694
5		9.816	-3.125	-4.984	-8.874	-2.101	3.194	-7.826
6		-23.58	26.376	10.252	12.13	-6.798	-3.402	19.069
7		68.029	3.338	7.905	2.815	-2.742	17.64	-32.332

6. Performance indicators

The performance of the C/R is characterised on the basis of the water desorption rate ($\dot{m}_{Des}$), which is the change in the amount of water evaporated from the weak solution, and therefore transferred to the air stream per unit time:

$$\dot{m}_{Des}=\dot{m}_{da}\cdot(\chi_{a,out}-\chi_{a,in}) \quad \text{(eq. 20)}$$

Where $\dot{m}_{da}$ is the mass flow rate of the dry air; $\chi_{a,out}$ and $\chi_{a,in}$ are the humidity ratios of the air at the top and bottom of the counter-flow sorption unit.

Finally, the average relative deviation (ARD) is selected as statistical indicator for comparing the results obtained from experiments ($P_{Exp[i]}$) and calculations ($P_{Mod[i]}$) (Qi et al., 2013):

$$ARD=(1/n)\cdot\sum_{i=1}^{n}\left|(P_{Exp[i]}-P_{Mod[i]})/P_{Exp[i]}\right|\cdot 100 \quad \text{(eq. 21)}$$

With n as the number of data set.

7. Results and discussion

The parity plot comparisons for the Nusselt and Sherwood numbers obtained from own experimental data and the literature data (Alizadeh and Saman, 2002; Li and Yang, 2010; Peng and Zhang, 2015, 2016) and the corresponding estimated from the coupled computational method are depicted in Fig. 3. The predicted Nusselt numbers exhibit a good fit to the experimental values, with an average relative deviation of ARD=12.7% and almost 90% of the data within the error bands of ±30% (R^2=0.98). On the other hand, approximately 94% of the Sherwood numbers estimated with the proposed correlation lie within the limits with ARD=10.5% (R^2=0.98). These results confirm the appropriate choice of the dimensionless groups used in the correlations to represent in a generalised and compact way the thermophysical properties of the fluids, temperature and mass concentration gradients between the liquid and gas phases, heat and mass transfer coefficients for the gas-phase, system geometry and other parameters that strongly influence the combined heat and mass exchanges in the regeneration of diluted desiccant solution within solar collector/regenerators.

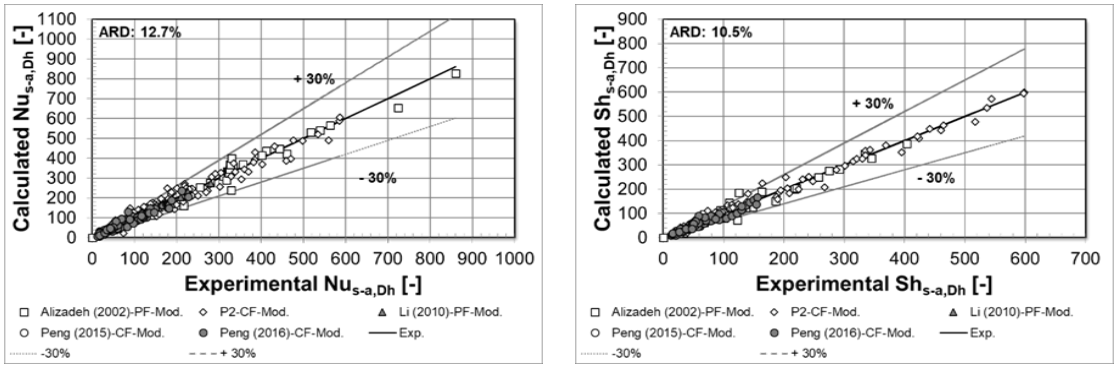

(a) Nusselt number (b) Sherwood number

Fig. 3: Comparison between calculated and experimental Nusselt and Sherwood numbers for simultaneous heat and mass fluxes in solar C/R.

Fig. 4 shows the parity plots between the water desorption rates determined from measurements in the test rig with aqueous $CaCl_2$ solution and those predicted from the new approach under the following boundary conditions: Global solar irradiance on the tilted collector varying between 925 and 1165 W/m²; air volumetric flow rate changing from 47 to 252 m³/h; inlet air temperature of about 32 °C; inlet air humidity ratio of approximately 12 g/kg; solution volumetric flow rate ranging between 4.8 and 30.1 l/h; inlet solution temperature of about 35 °C and inlet solution mass fraction of approximately 41%. The good matches achieved not only in the temperature changes of the liquid desiccant (ARD=8.3%) and air (ARD=11.8%) but also in the variations of the solution mass fraction (ARD=12.6%) and air humidity ratio (ARD=11.7%) at the inlet and outlet openings of the collector/regenerator contribute to enhance the accuracy of simulation by keeping the average relative deviation between the experimental and numerical values of the water desorption rate as low as 11.6% with almost 95% of the computations within uncertainty bands of ±30%.

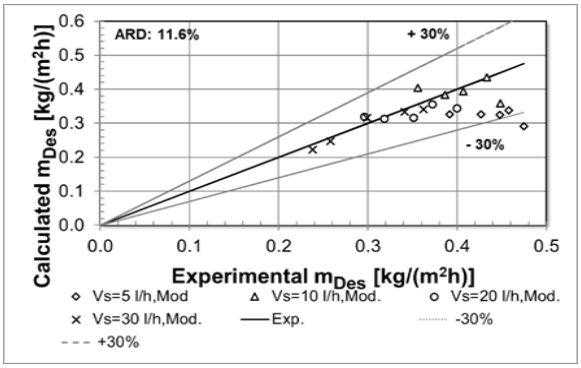

Fig. 4: Comparison between the calculated and experimental values of the water desorption rate obtained with the C/R prototype.

A group of experimental data reported by Peng and Zhang (2016) for a counter-flow solar C/R of 1 m width × 2 m length using aqueous LiCl solution has been selected for comparison with the numerical results obtained with the formulae derived by Peng and Zhang (2016) and by the authors of this work under following conditions: Global solar irradiance collected on the tilted plane varying between 419 and 786 W/m²; air volumetric flow rate changing from 69.8 to 350 m³/h; inlet air temperature fluctuating between 28.6 and 36.6 °C; inlet air humidity ratio ranging from 9.1 to 20 g/kg; solution volumetric flow rate varying between 12.1 and 18.1 l/h; inlet solution temperature changing from 24.8 to 31.6 °C and inlet solution mass fraction fluctuating between 23.7 and 25.7%. The model based on the expressions of Peng and Zhang (2016) gives a deviation of ARD=22.3% and keeps low dispersion against experimental data since all of its results are within error bands of ±30% (see Fig. 5(a)). However, the best outcomes are reached with the new correlations with a deviation of ARD=18.3% (see Fig. 5(b)). This can be explained by the inclusion of the coupled thermal and solutal buoyancy effects on the solution regeneration process in the collector channel through the heat and mass transfer Grashof numbers as well as the physical properties of the liquid sorbent through the Kapitza number in the new correlations, which improves the accuracy of the computed changes in the temperature and mass fraction of the desiccant solution.

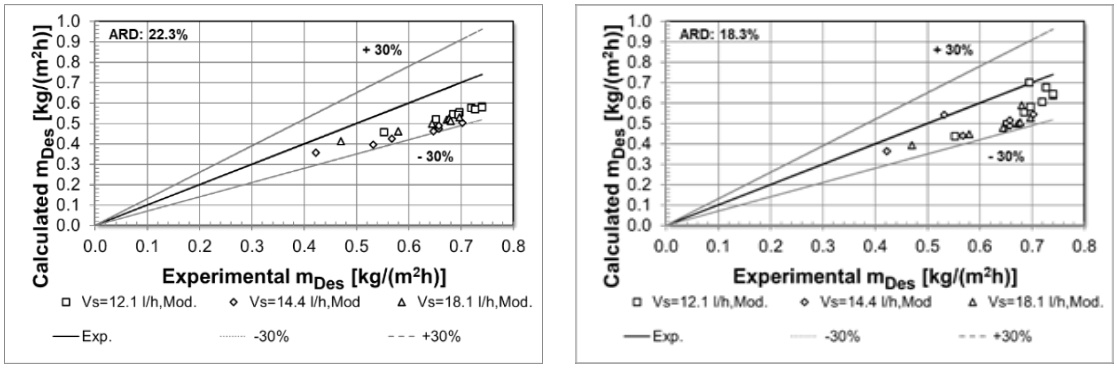

(a) Correlations of Peng and Zhang (2016) (b) Proposed correlations

Fig. 5: Comparison of the experimental water desorption rates reported by Peng and Zhang (2016) with the values predicted from the analysed formulations.

8. Conclusions

This paper presents new correlations for computing the Nusselt and Sherwood numbers in combined heat and mass transfer processes occurring in the regeneration of a liquid desiccant film flowing down the absorber plate of a solar collector/regenerator (C/R). These expressions were developed from measurements in the test rig using an aqueous solution of $CaCl_2$ with air flow in the turbulent regime and experimental data published in the literature using aqueous solutions of $CaCl_2$, LiBr and LiCl with air flow in the transitional and turbulent regimes.

The results show good agreements between the experimental and calculated values of the Nusselt and Sherwood numbers with average relative deviations of 12.7% and 10.5%, which demonstrates the suitability of the selected dimensionless groups for describing the simultaneous heat and mass fluxes occurring during the regeneration of weak solution within the device.

The coupled evaluation method of dimensionless convective heat and mass transfer coefficients is applied along with the energy and mass balances of the collector prototype in order to determine the water desorption rate of a diluted aqueous solution of $CaCl_2$ flowing in counter-current direction with air circulating through its channel. An average relative deviation of 11.6% is obtained for the water desorption rate under the analysed operating conditions due to the improved accuracy of the computations of the changes in the temperatures, mass fraction and humidity ratio of the fluids entering and leaving the C/R.

Further benchmarking is done to ascertain whether the new correlations developed in this work are more accurate than those proposed by Peng and Zhang (2016). For this purpose, experimental data published by Peng and Zhang (2016) for a counter-flow regenerating panel operating with aqueous LiCl solution are compared with the simulation results achieved from the above-mentioned formulations. Although the numerical results generated under the considered boundary conditions with both methodologies show low dispersion with respect to the experimental data, the computational model based on the new correlations provides the lowest average relative deviation with a value of 18.3%. In contrast, the mathematical model relying on the formulae of Peng and Zhang (2016) yields an average relative deviation equal to 22.3%. This is because the proposed methodology includes dimensionless groups that consider the combined effects of the thermal and solutal buoyancy forces and the physical properties of the liquid desiccant on the solution regeneration process.

The comparative analyses presented in this study have demonstrated the reliability and versatility of the new coupled evaluation method to simulate the simultaneous heat and mass exchanges taking place in the solar collector/regenerator when a liquid desiccant film is regenerated. Although this formulation is only valid for aqueous solutions of $CaCl_2$, LiBr and LiCl and air flow in the transitional and turbulent regions, it can be extended to other types of liquid sorbents and other air flow regimes by fitting it to newly available experimental data.

The new correlations developed in this work can be easily integrated into design or simulation programs to predict the thermodynamic performance of the solar collector/regenerator with high accuracy. This provides a good basis for future research aimed at analysing the technical and economic feasibility of direct solar regenerated liquid desiccant systems and evaluating measures for improving the heat and mass exchanges in a regenerating panel.

Acknowledgments

The funding provided by the Federal Ministry of Education and Research in framework of the program “Research at Universities of Applied Sciences-Funding Scheme Young Engineers” (contract number 03FH0041X4) during the initial stages of this research (2015-2018) is gratefully acknowledged.

References

Alizadeh, S., Saman, W. Y., 2002. An experimental study of a forced flow solar collector/regenerator using liquid desiccant. Solar Energy, 73(5), 345-362, DOI: 10.1016/S0038-092X(02)00116-0.

Cherif, A. S., Kassim, M. A., Benhamou, B., Harmand, S., Corriou, J. P., Jabrallah, S. B., 2011. Experimental and numerical study of mixed convection heat and mass transfer in a vertical channel with film evaporation. International Journal of Thermal Sciences, 50(6), 942-953, DOI: 10.1016/j.ijthermalsci.2011.01.002.

Enayatollahi, R., Nates, R. J., Anderson, T., 2017. The analogy between heat and mass transfer in low temperature crossflow evaporation, International Communications in Heat and Mass Transfer, 86, 126-130, DOI: 10.1016/j.icheatmasstransfer.2017.06.002.

Gnielinski, V., 2010. G2 Heat transfer in concentric annular and parallel plate ducts, in VDI Heat Atlas (2nd). Springer, Berlin, Heidelberg, pp. 701-708, DOI: 10.1007/978-3-540-77877-6_35.

Larachi, F., Levesque, S., 2008. Seamless mass transfer correlations for packed beds bridging random and structured packings. Industrial and Engineering Chemistry Research, 47(9), 3274-3284, DOI: 10.1021/ie070718o.

Li, Y., Yang, H., 2010. Experimental study of an open-cycle solar collector/regenerator using liquid desiccant for air conditioning. International Journal of Green Energy, 7(3), 273-288, DOI: 10.1080/15435071003796038.

Peng, D., Zhang, X., 2015. A modified model of solar collector/regenerator considering effect of the glazing temperature. International Journal of Refrigeration, 49, 151-159, DOI: 10.1016/j.ijrefrig.2014.10.004.

Peng, D., Zhang, X., 2016. Experimental investigation on regeneration performance, heat and mass transfer characteristics in a forced solar collector/regenerator. Energy, 101, 296-308, DOI: 10.1016/j.energy.2016.02.028.

Qi, R., Lu, L., Yang, H., Qin, F., 2013. Investigation on wetted area and film thickness for falling film liquid desiccant regeneration system. Applied Energy, 112, 93-101, DOI: 10.1016/j.apenergy.2013.05.083.

Taler, D., Taler, J., 2017. Simple heat transfer correlations for turbulent tube flow. E3S Web of Conferences, 13(4), DOI: 10.1051/e3sconf/20171302008.

Yang, R., Wang, P. L., 1994. Experimental study of a forced convection solar collector/regenerator for open-cycle absorption cooling. Journal of Solar Energy Engineering, 116(4), 194-199, DOI: 10.1115/1.2930081.